CORROSION SCIENCE AND TECHNOLOGY, Vol.18, No.1(2019), pp.1~7
[Research Paper]
pISSN: 1598-6462 / eISSN: 2288-6524
DOI: https://doi.org/10.14773/cst.2019.18.1.1

Effects of Surface Machining by a Lathe on Microstructure of Near Surface Layer and Corrosion Behavior of SA182 Grade 304 Stainless Steel in Simulated Primary Water

Zhiming Zhang, Jianqiu Wang†, En-hou Han, and Wei Ke

Laboratory of Nuclear Materials and Safety Assessment, Liaoning Key Laboratory for Safety and Assessment Technique of Nuclear Materials, Institute of Metal Research, Chinese Academy of Sciences, Shenyang 110016, P. R. C

(Received December 18, 2018; Revised January 17, 2019; Accepted January 23, 2019)

To find proper lathe machining parameters for SA182 Grade 304 stainless steel (SS), six kinds of samples with different machining surface states were prepared using a lathe. Surface morphologies and microstructures of near surface deformed layers on different samples were analysed. Surface morphologies and chemical composition of oxide films formed on different samples in simulated primary water with 100 μg/L O_2 at 310 °C were characterized. Results showed that surface roughness was mainly affected by lathe feed. Surface machining caused grain refinement at the top layer. A severely deformed layer with different thicknesses formed on all samples. In addition to high defect density caused by surface deformation, phase transformation, residual stress, and strain also affected the oxidation behaviour of SA182 Grade 304 SS in the test solution. Machining parameters used for # 4 (feed, 0.15 mm/r; back engagement, 2 mm; cutting speed, 114.86 m/min) and # 6 (feed,0.20 mm/r; back engagement, 1 mm; cutting speed, 73.01 m/min) samples were found to be proper for lathe machining of SA182 Grade 304 SS.

Keywords: *Surface machining, Cold-working, Microstructure, SS, Oxidation*

1. Introduction

Austenite SS has been widely used to fabricate the components of some main equipment in the nuclear power plants, owing to its favourable mechanical property and superior corrosion resistance. The surface states of the mechanical parts are closely related with the manufacture processes. In practice, the surface roughness is often selected as the key parameter to control the surface finish between the two neighbouring steps. The choice of the specific machining parameters for a mechanical part is nearly relied on the workers. Limited to the man-hours and practical experiences, the choice of the parameters is of great randomness. This will result in a fact that the mechanical parts with the same or similar surface roughness may have different surface cold-worked layer. As a result, the microstructure of the near surface deformed layers, such as hardness, the residual stress or strain, as well as grain size can be very complex. Further, this may affect the corrosion of SS dramatically in the later practical service environment.

Ghosh *et al.* had studied the corrosion of the machined, ground and solution annealed SS [1-3]. It was found that the surface machining could cause the grain refinement in the surface cold-worked layer. More Cr atoms were found in the oxide films formed on machined and ground surfaces, compared with the solution annealed ones. The surface deformation seemed to be beneficial to increase its oxidation resistance. However, the surface machining increased the stress corrosion cracking sensitivity dramatically of the SS in terms of the time of initiation of the cracks.

Although the effects of surface machining on the corrosion behaviour have been evaluated, to date, fewer papers have studied the selection of the machining parameters on the corrosion of SS. The optimization of the machining parameters will be more important in practice, as it will be expected when a machined surface with good surface finish also shows the least surface deformation but superior corrosion resistance. Further, this can directly guide the actual machining operations in the factory. The purpose of this study is to clarify the relationship between the surface machining by different operation parameters and the microstructures of the near surface layers, as well

† Corresponding author: wangjianqiu@imr.ac.cn

Table 1 Chemical composition of SA182 Grade **304 (wt%)**

C	Mn	P	S	Si	Cr	Ni	N	Fe
0.053	1.59	0.022	0.004	0.47	18.45	8.30	0.057	Balance

Table 2 The specific machining parameters of 6 kinds of samples by lathe

No.	Feed (mm/r)	Feed speed (mm/min)	Back engagement (mm)	Cutting speed (m/min)
1#	0.5	2.92	1	170.35
2#	0.5	1.25	1	73.01
3#	0.15	1.06	2	206.85
4#	0.15	0.59	2	114.86
5#	0.20	1.33	1	194.68
6#	0.20	0.50	1	73.01

as the corrosion behaviour differences. As a conclusion, the proper machined parameters for SA182 Grade 304 SS will also be proposed.

2. Experimental Procedure

2.1 Materials and sample preparation

The samples used in the experiments were cut from one solution annealed SA182 Grade 304 SS ingot with 155 mm in diameter. Its chemical composition is listed in Table 1. To study the effects of machining operation on the microstructures of the near surface deformed layers, the end surface of the ingot was machined by a lathe with different machining parameters, such as the feed speed, the cutting speed and the back engagement. Thus, 6 kinds of samples with different surface state were prepared in the present study. The specific machining parameters for every kind of specimen are shown in Table 2. In the following, 1#, 2#, 3#, 4#, 5# and 6# were used to denote different samples, as shown in Table 2. For the microstructure characterization of different samples, 6 entire end surfaces with 3 mm in thickness were first cut from the ingot and sample coupons were then cut into sizes of 15 mm by 15 mm from these sheets. All samples were then washed with acetone, ethanol, and deionized water.

2.2 Microstructural characterization of near surface cold-worked layers by surface machining

The surface profiles of these prepared samples were observed using an FEI XL 30 scanning electron microscope (SEM). Surface roughness of the samples was measured using a LINKS 2205 surface profilometry. Every kind of surface was measured for 2 – 3 times and the scanning direction of the detector probe was parallel to the feeding direction.

The cross section of the machined samples which was parallel to the feeding direction was ground to 2000 grit with waterproof silicon carbide abrasive paper and then mechanical polished to 1.5 μm with diamond paste. The grain structure in the surface deformed layer was investigated by electron backscattered diffraction (EBSD) measurements. After ultrasonic cleaned in alcohol, the cross section was then polished manually with 20 nm SiO_2 suspension. The EBSD measurements were performed on the SEM with TexSemLaboratories,Inc. (TSL) EBSD equipment. The step size of 0.2 μm was used in the measurement. A commercially available TSL orientation image microscopy (OIM) software was used to analyse the EBSD results.

2.3 Immersion test

The immersion test was performed in a 7L type 316L SS autoclave with a water circulating loop. 1500 ppm B as boric acid (H_3BO_3) and 2.3 ppm Li as lithium hydroxide monohydrate ($LiOH•H_2O$) were added into the deionized water to simulate the primary water. The dissolved oxygen in the water tank was controlled to be 100 μg/L and the dissolved hydrogen was less than 1μg/L for this experiment. The immersion test was performed at 310 °C and 11 MPa for 498 h.

After immersion test, the surface morphology of the oxide films formed was examined by the above SEM. The chemical composition of the oxide films was analysed using X-ray photoelectron spectroscopy (XPS) ESCALAB250 with Al Kα radiation (hν = 1486.6 eV) at a pass energy of 50.0 eV. The take-off angles of photoelectrons was 45°, with respect to the sample surfaces. In order to get the composition-depth profiles by successively removing the oxide surface with argon ion bombardment, a 2 keV argon ion sputtering at a target current of 2 $\mu A/cm^2$ and a pressure of 5.5×10^{-8} mbar was used.

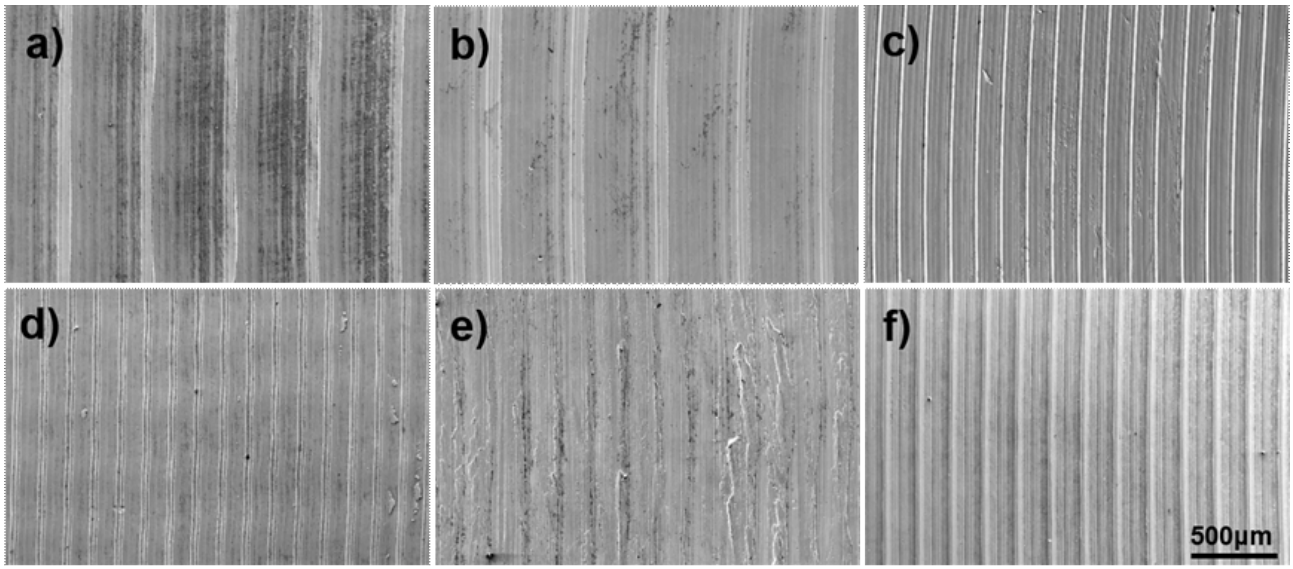

Fig. 1 SEM images showing surface morphologies of SA182 Grade 304 SS samples with different machining surface states by SEM: (a) 1#; (b) 2#; (c) 3#); (d) 4#; (e) 5#); (f) 6#.

3. Resutls and Discussion

3.1 Surface morphology observation before immersion

Figs.1a–f show the surface morphologies of different samples before immersion by SEM. The surfaces of all samples are covered with the parallel grooves formed during the machining operation. The observed grooves are perpendicular to the feeding direction. The depth and width of these grooves on different samples are of great difference, which are dramatically dependent on the machining parameters. It can be seen that the width of the grooves are determined by the lathe feed. The surface texture formed during the lathe feeding on the samples in Figs. 1a–d and 1f, are regular, except the 5# sample in Fig. 1e, where the distribution of surface grooves seems to be orderless and parts of some grooves are destroyed by the lathe tool during machining operation. Thus, the surface state of 5# sample is worst among the test samples. Meanwhile, it can be seen that the 5#, 1# and 2# samples are much wavier than 3#, 4# and 6# samples, which is consistent with the results of surface roughness measurement in Fig. 2. For the surface roughness, it is biggest for the samples 1# and 2#, the following is 5# and it is smallest for the sample 4#. The roughness of samples 3# and 6# is a little bigger than that of 4# sample. As the surface texture of 5# sample is irregular, the measured roughness values of this sample are of great dispersity. However, the roughness values measured for several times are nearly the same for the each sample of the rest ones, indicating the surface topography of these samples are uniform.

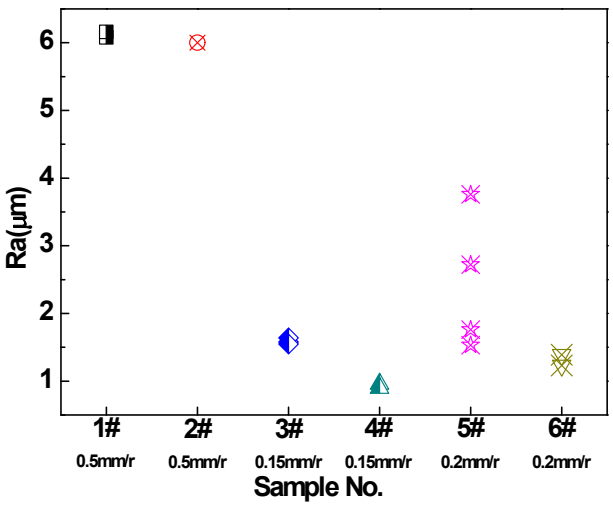

Fig. 2 Surface roughness values of SA182 Grade 304 SS samples with different machining surface states.

According to the surface morphology observation and roughness measurement, it can be found that the surface roughness are mainly related with the lathe feed, in general, when the cutting speed and the back engagement are controlled to be similar or the same, respectively, the bigger the feed, the rougher the surface. For the samples with the same feed (0.5 or 0.15 mm) and back engagement (1 or 2 mm), such as 1# and 2# samples or 3# and 4# samples, the used cutting speed can hardly affect the surface roughness. However, for the samples 5# and 6# with the same feed of 0.2 mm, when the back engagement are

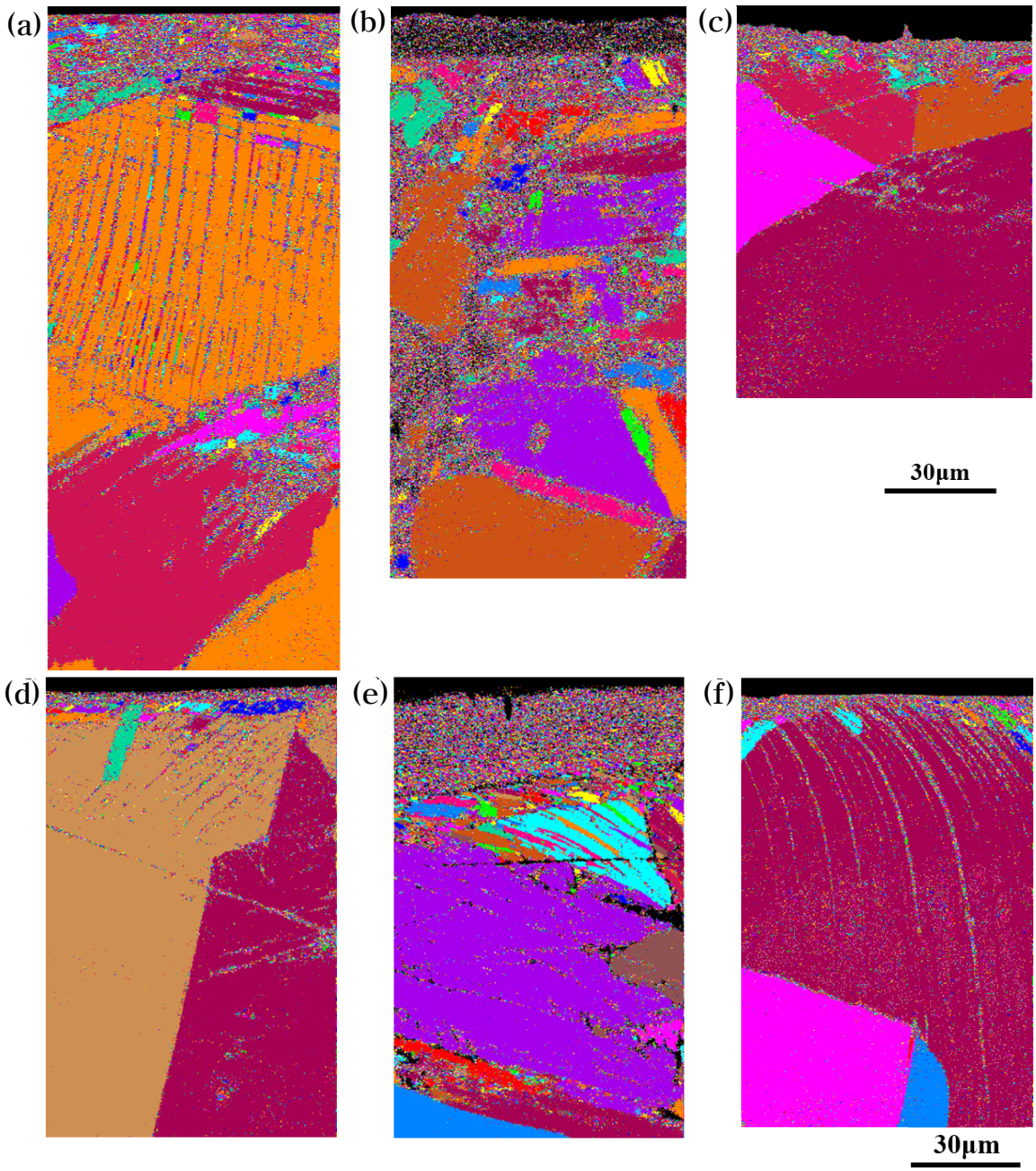

Fig. 3 Grain images of near surface deformed layers of samplers with different surface states: (a) 1#; (b) 2#; (c) 3#); (d) 4#; (e) 5#); (f) 6#.

the same, the cutting speed can affect the surface roughness dramatically. It can deteriorate the surface topography or the surface finish severely, when the cutting speed is bigger than 194.68 m/min.

3.2 Cross-sectional EBSD measurement

Fig. 3 shows the results of the cross-sectional EBSD measurement of 6 kinds of analysed samples. Figs. 3a–f are the grain images of the near surface layers in different samples. A surface deformed layer by lathe machining is formed on each kind of sample. It can be seen clearly that the severe deformation has caused the grain refinement of the top layer. According to the grain size, the surface deformed layer shows a characteristic of gradient structure in the depth direction and can be divided into 3 layers. The outmost layer with the severest deformation is composed of nano-sized grains, of which the grain size is less than 100 nm. Increasing the depth, the level of

the deformation decreases and the grain size of the deformed grains increase gradually. The intermediate layer is composed of grains of about 10–20 μm in size. When approaching the matrix free of strain or deformation, the grains in the third layer is full of slip bands or mechanical twins and the grain size is not changed. The surface deformed layers on different samples show a similar layered structure. The nano-sized deformed layer observed in the present study is consistent with the published results [1-3]. The formation of the surface nano-sized layer can be ascribed to the fast strain rate and the high strain by the lathe machining. The phase identification by EBSD also showed that the top layer was composed of martensite, indicating the surface austenite structure had been transformed into the martensite by the severe deformation [1-3].

If the depth where the slip bands disappear at the cross section is considered as the matrix free of deformation,

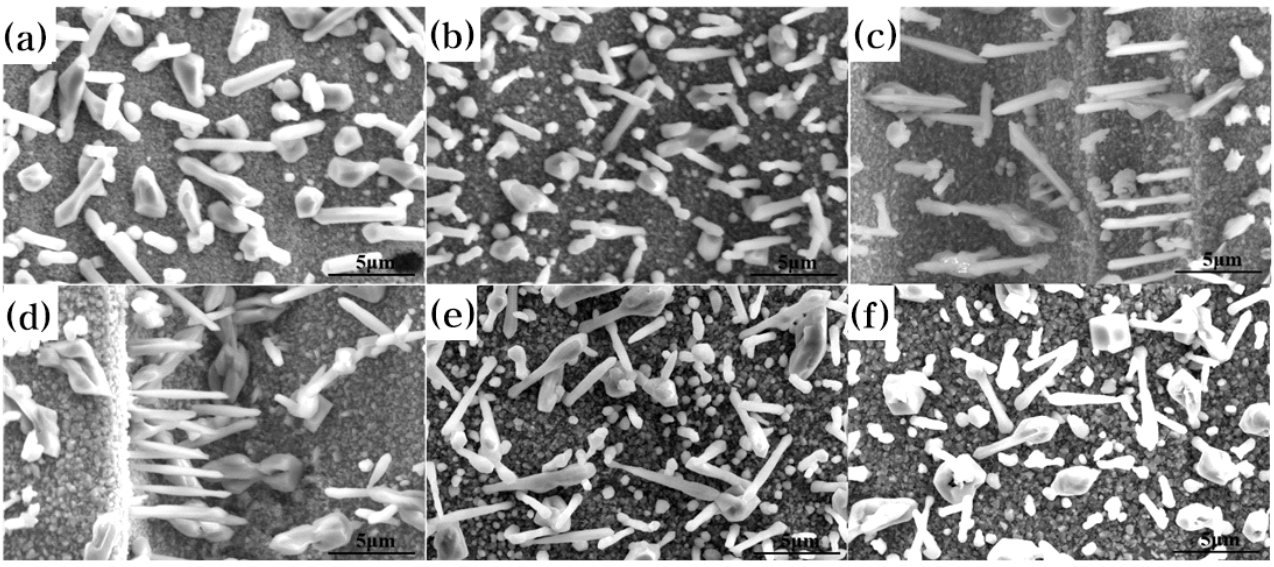

Fig. 4 Surface morphologies of oxide films formed on SA182Grade 304 SS samples with different machining surface states after immersion in simulated primary water with 100 μg/L O_2 at 310 °C and 11 MPa for 498 h.

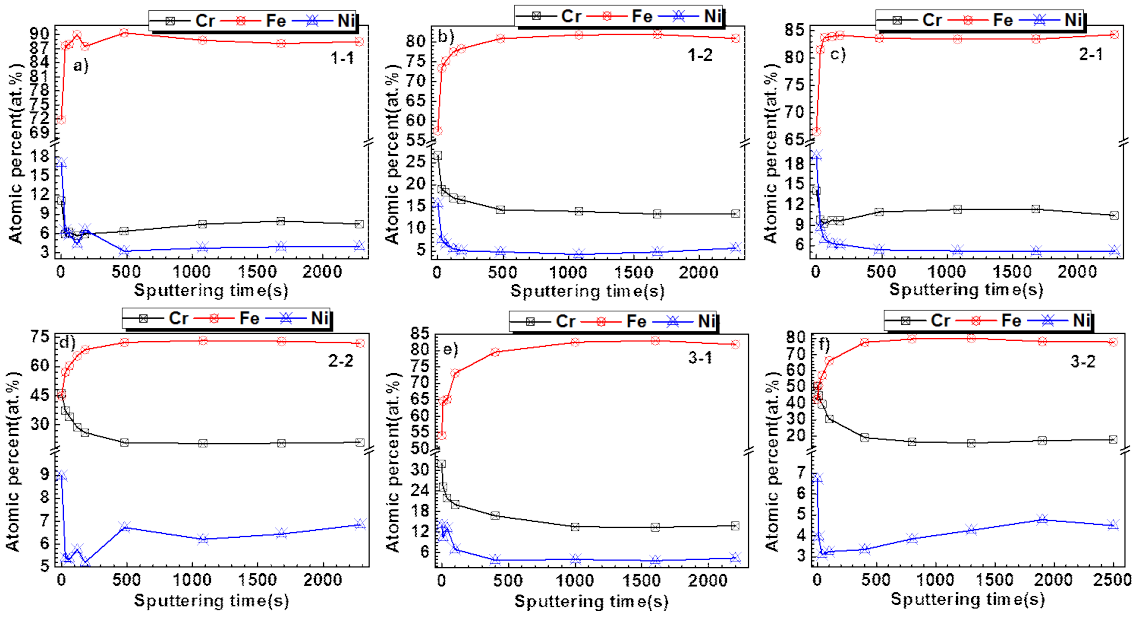

Fig. 5 Chemical composition of oxide films formed on SA182Grade 304 SS samples with different machining surface states by XPS after immersion in simulated primary water with 100 μg/L O_2 at 310 °C and 11 MPa for 498 h.

the thickness of the surface deformed layers on different samples can also be estimated from the cross-sectional grain images, which is about 150, >150, 80, 80, >130 and 100 μm for the 1#, 2#, 3#, 4#, 5# and 6# samples, respectively. As the scanning area by EBSD is relatively small, Figs. 3b and e only shows part of the deformed layers on 2# and 5# samples.

Further comparing the surface deformed layers on different samples, it is found that the thickness of every layer is different, respectively. The surface deformed layer and the outmost layer with nano-sized grains on the 5#, 1# and 2# sample are thickest, indicating the deformation level of the 5#, 1# and 2# samples is severest.

Figs. 4a–f show the surface morphologies of oxide films grown on SA182Grade 304 SS samples with different surface states after immersion in simulated primary water with 100 μg/L O_2 at 310 °C and 11 MPa for 498 h. It is similar for the oxides grown on samples with different surface states. According to the surface appearance of the oxides, the oxides formed can be classified into two groups: the outmost big oxide particles with irregular shape and the rod-like oxides, the underlying compact well-formed small oxide particles. Therefore, the surface state cannot affect the surface morphology of the oxides formed on SA182 Grade 304 SS in the studied solution. Figs. 5a–f depict the absolute chemical composition of the oxide films grown on SA182Grade 304 S samples with different surface states after immersion test. As the oxide film formed on the sample surfaces are very thick, the successive-sputtering by argon ions was only performed for about 2500s. In order to compare the chemical composition of the surface oxide film with that of the matrix, the O content in the results is excluded. It is obvious that the oxide films formed on all test samples are rich in Fe and the Ni content in the oxide films is lowest. Further, the Cr content in the oxide films grown on different samples is distinctly different. For the 6# and 4# samples, the Cr content at the top layer reaches about 45–50 at%. Increasing the sputtering time, the Cr and Ni contents in the oxide films decrease gradually, whereas the Fe content increase gradually. After sputtering for about 2500s, the Cr content decrease to about 20 – 25 at%, which is still higher than that of the matrix. Thereby, a Cr-rich oxide film is formed on the 6# and 4# samples. The Cr content at the top layer in the oxide films formed on the 2# and 5# samples is about 25 – 30 at%. After sputtering for about 2500s, the Cr content decreases to about 15 at%. By comparison, the Cr content in the oxide films formed on the 1# and 3# samples is lowest.

It has been calculated that the open circuit potential of SS in the present primary water with 100 μg/L O_2 at 310 °C is about -250–-50 mV (SHE) [4]. According to the pH-potential diagrams of Ni-H_2O, Cr-H_2O and Fe-H_2O at 300 °C [5], the stable forms of Ni, Cr and Fe are NiO, Cr_2O_3 and Fe_3O_4. Kim has studied the corrosion of 304 SS in the pure water with 200 μg/L O_2 at 288 °C [6,7]. The surface oxide film formed is composed of an outer layer with Fe_2O_3 and an inner layer with $FeCr_2O_4$ and Fe_3O_4. The chemical composition in Figs. 5a–f indicates the oxide film formed in the present study is also composed of the similar oxide phases, but doped with small amount of Ni atoms and excessive Cr atoms, when considering the similar water chemistry condition. As a result, the Cr-rich oxides, such as $(Fe, Cr)_2O_3$ and $(Ni, Fe)Cr_2O_4$, are formed after immersion in the water containing B and Li at 310 °C. Further, the Cr atoms in the matrix can be oxidized and then stabilized in the surface oxide films. It is agreed well that the Cr-rich oxide film can suppress the diffusion coefficient of metallic and oxygen atoms and then can protect the matrix from further corrosion [1,8]. Thus, the oxide films formed on the 6# and 4# samples are most protective, the following are the oxide films formed on the 2# and 6# samples and the oxide film formed on the 1# and 3# samples are least protective.

Ghosh *et al.* had studied the effects of surface working operations on the high temperature oxidation behavior of 304L ss in the high purity water with the dissolved O concentration in the inlet water lower than 5 ppb (by mass) at 300 °C and 10 MPa [1]. Compared with the solution annealed samples, surface machining results in extensive grain refinement, strain induced martensite transformation and high magnitude of plastic deformation near the surface. Moreover, surface machining and grinding caused the changes in the oxidation behavior of SS. The oxides formed on the machined and ground surfaces had higher specific resistivity and more Cr was found in these oxide films. The thickness of the oxide film formed on the solution annealed surfaces was the highest, which was followed by the oxides films formed on the machined and ground surfaces. It was discussed that the differences in the oxidation behavior were attributed to the occurrence of the grain refinements in the surface deformed layers and the martensitic phase formed by machining and grinding operations. Thus, it is deduced that the high density grain boundaries, subgrain boundaries and dislocations caused by the grain refinement in the near surface deformed layers may act as the short-cuts for the inward diffusion of O atoms and also for the outward diffusion of metallic atoms from matrix. The surface cold-working by machining and grinding is thought to be beneficial for the growth of the surface protective oxide film.

Whereas this seems to be inconsistent with the present

results in Figs. 3 and 5. EBSD analysis in Figs. 3a–f shows that the surface deformed layer and the surface layer with nano-sized grains on the 5#, 2# and 1# samples are thickest and the surface deformed layers on the 4#, 3#, and 6# samples are much thinner. However, the chemical composition in Figs. 5a–f indicates the Cr atoms in the oxide film formed on the 5#, 1# sample are not richest. By comparison, the Cr atoms in the oxide films formed on the 4#, 6# and 2# samples are richest. Thus, in addition to the surface high density defects, the other factors, such as the phase transformation, residual stress/strain, even the surface roughness should also be evaluated when discussing the effects of surface cold-working on the oxidation behavior of SS in the high temperature water. The near surface microstructure differences between the used 6 kinds of samples will be further characterized to find out the root cause of the oxidation behavior differences.

In the present study, the surface roughness and the thickness of surface deformed layer on the 4# and 6# samples are lowest, meanwhile, the oxide films formed on these samples are most protective. Therefore, the machining parameters of the 4# and 6# samples are suggested to be proper for the lathe machining of the used SA182 Grade 304 SS.

4. Conclusions

6 kinds of SA182Grade 304 SS samples with different machining surface states were prepared by a lathe. The surface morphologies and the microstructures of the near surface deformed layers on different samples were characterized. The surface morphology and chemical composition of the oxide films formed on different samples were analysed. The following conclusions could be drawn from the present results.

(1) The surface roughness were mainly affected by the lathe feed. A severely deformed layer with nano-sized grains at the top layer was formed on all samples.

(2) In addition to the high density defects caused by the surface deformation, the phase transformation, residual stress and strain should also be discussed when studying the effects of surface machining on the oxidation behaviour of SS in the high temperature water.

(3) The machining parameters for the 4# (feed-0.15 mm/r, back engagement-2 mm, cutting speed-114.86 m/min) and 6# (feed-0.20 mm/r, back engagement-1 mm, cutting speed-73.01 m/min) samples were suggested to be proper for the lathe machining of the used SA182 Grade 304 SS.

Acknowledgments

This work was supported by the National Key Research and Development Program (2017YFB0702100), Open-Ended Fund of Key Laboratory of Nuclear Materials and Safety Assessment, Institute of Metal Research, Chinese Academy of Sciences (2016NMSAKF01), National Natural Science Foundation (No. 51301183) and Research Fund for the Doctoral Program of Liaoning Province (No. 20131119).

References

1. S. Ghosh, M. K. Kumar, V. Kain, *Appl. Surf. Sci.*, **264**, 312 (2013).
2. S. Ghosh, V. Kain, *J. Nucl. Mater.*, **403**, 62 (2010).
3. S. Ghosh, M. K. Kumar, V. Kain, *Adv. Mat. Res.*, **794**, 564 (2013).
4. H. L. Ming, Z. M. Zhang, S. Y. Wang, J. Q. Wang, E.-H. Han, W. Ke, *Mater. Corros.*, **66**, 869 (2015).
5. R. W. Staehle, J. A. Gorman, *Corrosion*, **59**, 931 (2003).
6. Y. J. Kim, *Corrosion*, **55**, 81 (1999).
7. Y. J. Kim, *Corrosion*, **56**, 389 (2000).
8. M. S. Li, *High Temperature Corrosion of Metals*, *1st ed.*, p. 184, Metallurgical Industry Press, Beijing (2001).